analytical chemistry

pubs.acs.org/ac Article

Electrochemical Deposition of Cu Metal−Organic Framework Films for the Dual Analysis of Pathogens

Zhaowei Sun, Ying Peng, Minghui Wang, Yuxin Lin, Mohammed Jalalah, Saeed A. Alsareii, Farid A. Harraz,* Jie Yang, and Genxi Li*

Cite This: *Anal. Chem.* 2021, 93, 8994−9001 Read Online

ACCESS | Metrics & More | Article Recommendations | Supporting Information

ABSTRACT: Metal−organic framework (MOF) thin films with flexible nature and prominent qualities have opened doors to new technological applications in different fields. Herein, we propose an electrochemical biosensor for the dual detection of Staphylococcus aureus based on the electrodeposition of Cu metal−organic framework (Cu-MOF) thin films. The promising sensing layer with features of good electronic conductivity and enhanced electron-transfer property can not only identify *S. aureus* through specific micrococcal nucleases in the supernatant but also detect the pathogen directly *via* aptamer recognition. The dual analysis design ensures the accuracy of this method for *S. aureus* detection in the range of 7−7 × 10^6 cfu/mL with the limits of detection of 1.9 and 5.2 cfu/mL. Moreover, the analytical method validation confirmed that the biosensor could efficiently work in complex biological samples, showing good selectivity and specificity and great potential for clinical diagnosis. More importantly, the current proposed strategy is simple and easy to implement without the need for extra signaling elements, which is convenient for timely clinical detection.

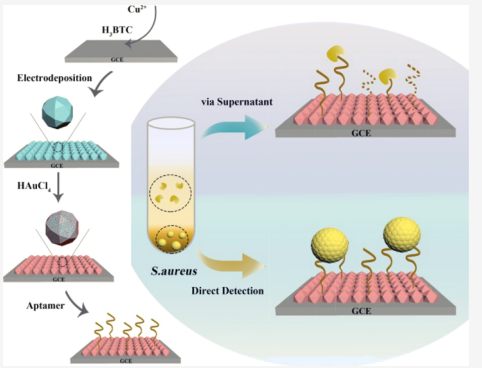

Metal−organic frameworks (MOFs) have emerged as a unique kind of inorganic−organic hybrid nanomaterial, which has been widely used in many fields due to the characteristics of uniform structure, chemical tenability, and good biocompatibility.[1−7] Recently, MOF thin films with large surface areas, flexible nature, and prominent qualities have opened doors to new technological applications in various fields.[8−10] Nevertheless, the application of MOF films in the development of electrochemical biosensors remains a challenge due to their poor electrical conductivity.[11,12] Earlier studies have reported that their electrical conductivity can be improved by introducing redox-active metal ions or electroactive conjugated organic ligands,[13] such as Cu^{2+} and Ni^{2+} metal salts as well as ligands of terephthalate and 1,3,5-benzenetricarboxylate,[14−16] which may greatly expand the utilization of MOF films. Moreover, with the increase in demand, the formation techniques of MOF films have been developed rapidly, such as seeded growth, dip- or spin-coating, Langmuir−Blodgett layer-by-layer deposition, and chemical vapor deposition.[17−22] However, most of them are of multisteps, complex, time-consuming, and highly demanding with low practicability and reproducibility. Electrochemical deposition can be used as an alternative and efficient approach for the MOF-film preparation, which can be formed *in situ* on the electrode surface under mild conditions. More importantly, the electrochemical deposition procedure is rapid, efficient, easy, and can be precisely controlled.[23,24] Inspired by these salient characteristics, MOF films prepared by electrodeposition are designed in this work for the fabrication of an electrochemical biosensor, which can be applied for the dual analysis of pathogens.

Pathogenic infections have become an increasingly serious problem worldwide, especially the diseases caused by drug-resistant bacteria, as a result of indiscriminate and excessive use of antibiotics in medical and agricultural fields.[25−27] For example, methicillin-resistant *Staphylococcus aureus* (MRSA), which was observed first in 1960 and has been spreading rapidly in the globe since the 1990s, has become one of the main causes of hospital infections now.[28−32] It is reported that drug-resistant bacterial infections have led to severe deaths annually, and the mortality is predicted to be 10 million by 2050 if immediate action is not taken.[33,34] Additionally, owing to the delay in the detection and treatment of pathogens, the conditions of patients will deteriorate rapidly after the onset of symptoms.[35] The treatment usually involves systemic injection of large amounts of antibiotics, which damage the innate immune system and maybe result in the evolution of drug-resistant bacteria.[36,37] Therefore, it is indispensable to develop

Received: April 26, 2021
Accepted: June 11, 2021
Published: June 21, 2021

https://doi.org/10.1021/acs.analchem.1c01763
Anal. Chem. 2021, 93, 8994−9001

Scheme 1. (I) Fabrication of the DNA/AuNPs/MOFs-Based Sensing Platform; (II) Schematic Diagrams of the Electrochemical Biosensor for the Detection of *S. aureus via* Supernatants; and (III) Pathogen Cells

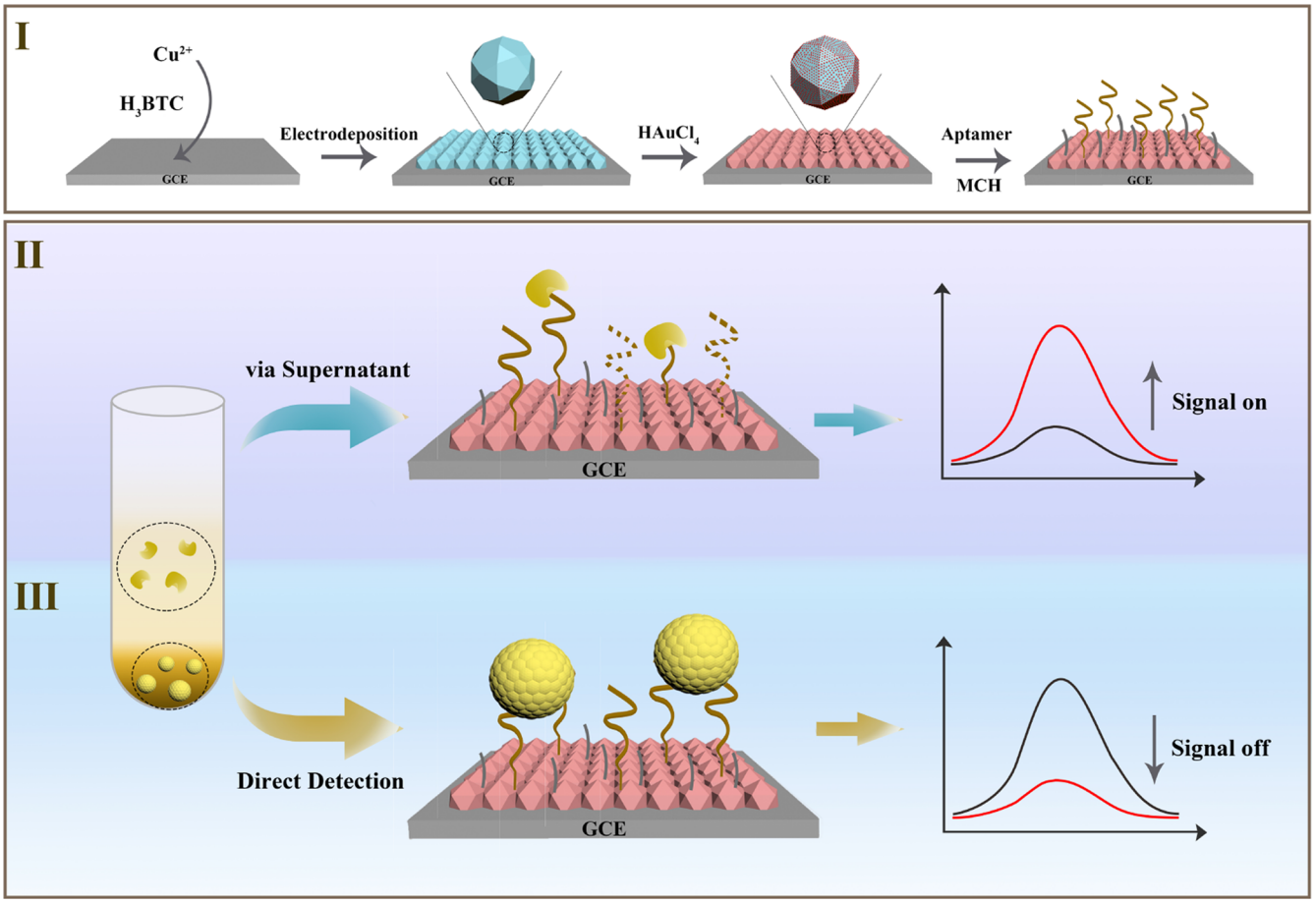

rapid and efficient methods to detect pathogens of infectious diseases for the timely and appropriate guidance for antibiotic usage and treatment of patients. Compared with conventional methods such as culturing,[38] DNA-based polymerase chain reaction (PCR),[39] and immunosorbent assays,[40] electrochemical techniques have attracted more and more interest because of their rapid response, sensitivity, convenience, and simplicity.[41]

Taking the above considerations into account, we have developed an electrochemical biosensor based on the electrodeposition of Cu-MOF films for the dual quantitative analysis of *S. aureus*. *S. aureus* is selected for this work because it is a major pathogen in human diseases and is an example of methicillin-resistant pathogens. As depicted in Scheme 1, under a negative potential, conductive Cu-MOFs are directly self-assembled and deposited onto the electrode surface in the presence of copper ions and the conjugated ligands, enhancing the rate of redox-active molecules reaching the electrode surface.[20,42] Then, gold nanoparticles (AuNPs) are reduced *in situ* on the MOF surfaces to form a composite material, which can further enhance the electron transfer and bind to aptamers *via* the Au−S bonds. Hence, the composition films of AuNPs/MOFs conjugated with a DNA aptamer (DNA/AuNPs/MOFs) may offer a promising platform for the fabrication of an electrochemical biosensor. When the *S. aureus* exists, the pathogen can specifically secrete a micrococcal nuclease (MNase) in the supernatant, which can digest single- or double-stranded, round or linear nucleic acids by cleaving the phosphodiester bonds.[43,44] After incubating with the supernatant solution, the DNA aptamer on the surface of the electrode will be cut down and then the electrochemical signals of $[Fe(CN)_6]^{3-/4-}$ in the test solution will increase. Therefore, the strategy can identify the *S. aureus* through the supernatant of bacterial culture. Meanwhile, MNase is conserved in different strains, which can be used as a biomarker for the evaluation of the pathogenicity of *S. aureus*.[45−47] Additionally, the DNA/AuNPs/MOF-sensing interface can also detect the pathogen directly through specific molecular recognition. The aptamer can selectively recognize *S. aureus* cells and pull them to the electrode surfaces, leading to higher interfacial impedance and preventing the redox-active molecules in the solution from reaching the electrode surface due to the high insulation and negative charge of the pathogen surface.[48,49] As a result, the electrochemical signals of $[Fe(CN)_6]^{3-/4-}$ in solution will reduce in the presence of *S. aureus*.

EXPERIMENTAL SECTION

Materials and Instrumentation. Details are given in the Supporting Information section.

Microbial Culture. *Escherichia coli*, *S. aureus*, and *Listeria monocytogenes* were cultured in lysogeny broth (LB) medium, shaking at 200 rpm at 37 °C for 12 h; afterward, the bacterial culture was diluted with PBS or urine. The microbial cells or supernatants were harvested by using centrifugation at 12,000 rpm and 4 °C, and the microbial cells were washed twice with PBS. The microbial content was calculated by the plate

https://doi.org/10.1021/acs.analchem.1c01763
Anal. Chem. 2021, 93, 8994−9001

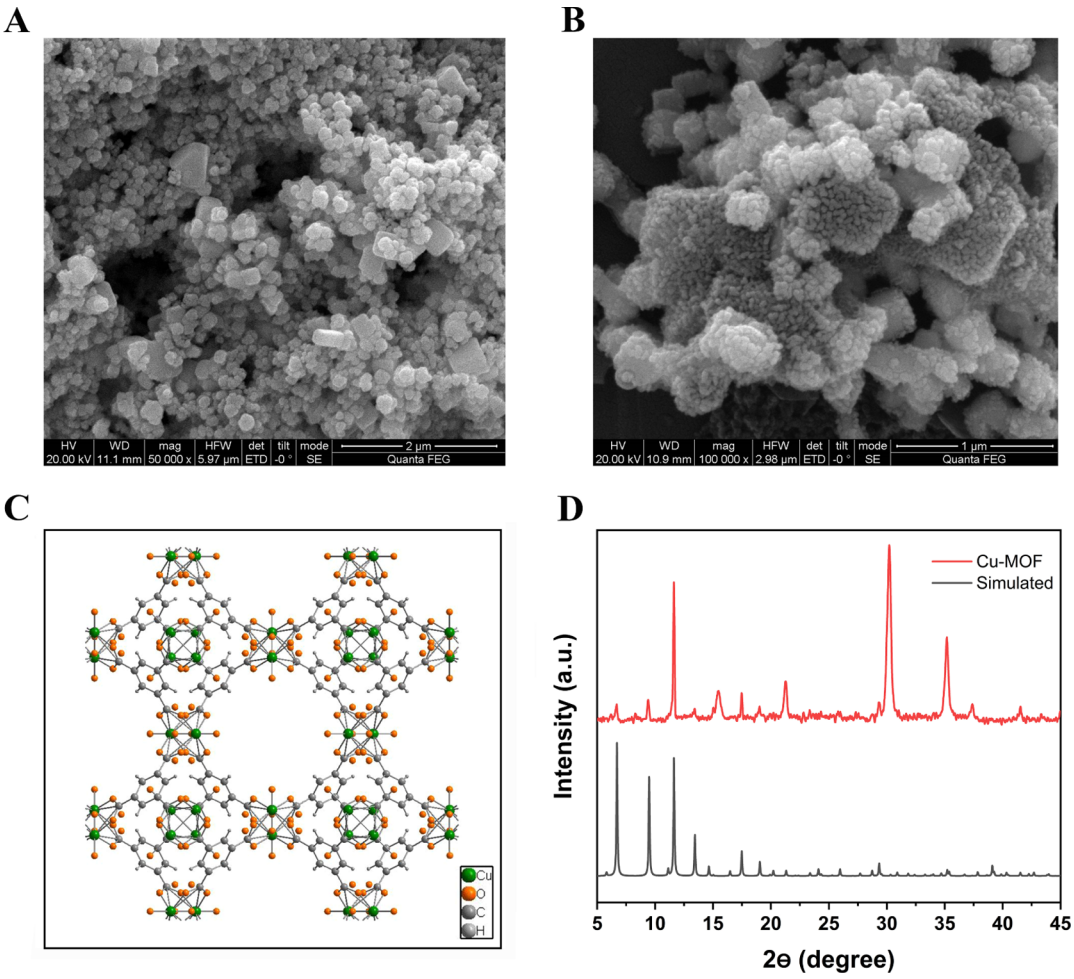

Figure 1. SEM images of the (A) Cu-MOFs and (B) AuNPs/Cu-MOFs on the electrode surface. (C) Crystalline structures of Cu-MOFs. (D) Powder XRD patterns of both simulated and synthesized Cu-MOFs.

counting method. The bacterial culture was diluted 1000 times by LB medium and then 10 μL was taken out for culture at 37 °C for 12 h, and the number of single colonies was.

For urine sample analysis, the microbial cells or supernatants were first harvested or collected and diluted with human urine. Then, the fabricated biosensor was used to detect the samples.

Treatment and Modification of the Electrode. The bare glassy carbon electrode (GCE, 3 mm in diameter) was first polished with 1, 0.3, and 0.05 μm alumina slurry in sequence similar to our previous work.[50] After ultrasonic treatment in ethanol and distilled water for 5 min, the electrode was rinsed and dried with high-purity nitrogen.

For the electrodeposition of Cu-MOF films, the cleaned electrode was immersed in the precursor solution, containing a cationic source ($Cu(NO_3)_2{\cdot}3H_2O$, 10 mM), an organic linker (H_3BTC, 15 mM), and a probase source (Et_3NHCl, 10 mM) in DMF at a potential of −1.30 V for 5 min. The resulting electrode was swiftly taken out and dried at 50 °C to achieve a Cu-MOF film-modified electrode. Then, the modified electrode was immersed in 5 mM $HAuCl_4$ solution for the AuNP reduction on the Cu-MOF surfaces at −0.5 V for 30 s, forming a composite film of AuNPs/MOF on the electrode.

Biosensor Fabrication. The prepared AuNPs/MOFs/GCE was incubated with a 0.5 μM designed aptamer (SH-DNA), which was reduced by 1 mM tris(2-carboxyethyl) phosphine in advance for 30 min at 37 °C. After rinsing and drying with nitrogen, the electrode was incubated with 1 mM 6-mercapto-1-hexanol for 30 min to block the blank sites and exclude unspecific adsorption. After rinsing, the DNA/AuNPs/MOFs-based electrode was incubated with different concentrations of bacteria or supernatant at 37 °C for the target reaction. Finally, the electrode after target recognition was carefully cleaned and is ready for electrochemical measurements.

Electrochemical Measurements. A CHI660D potentiostat with a conventional three-electrode system was used to perform electrochemical measurements, for which the working electrode was the AuNPs/MOFs/GCE modified with aptamers, the reference electrode was a saturated calomel electrode, and the counter electrode was a platinum wire. The electrochemical impedance spectroscopy (EIS) measurements were recorded in $[Fe(CN)_6]^{3-/4-}$ (5 mM) electrolyte containing KCl (1 M). The detailed experimental parameters were an amplitude of 5 mV, a bias potential of 0.224 V, and a frequency range of 0.1−10 kHz. Cyclic voltammetry (CV) scan was performed from −0.2 to 0.6 V in KCl (0.1 M) solution with a 0.1 V/s scan rate. Differential pulse voltammetry (DPV) measurements were carried out, for which 50 mV/s sweeping rate, 50 ms pulse width, 0.2 s pulse period, and voltage range from −0.2 to −0.6 V were used as experimental parameters.

https://doi.org/10.1021/acs.analchem.1c01763
Anal. Chem. 2021, 93, 8994−9001

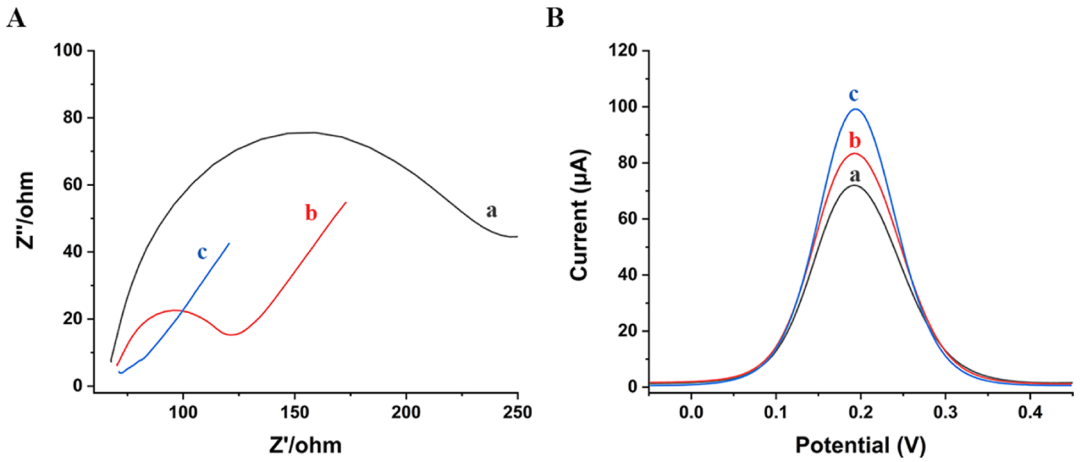

Figure 2. (A) EIS spectra and (B) DPV curves corresponding to different treatments of the electrodes. Curves (a–c) represent, respectively, the cases of the bare GCE, MOFs/GCE, and AuNPs/MOFs/GCE electrodes.

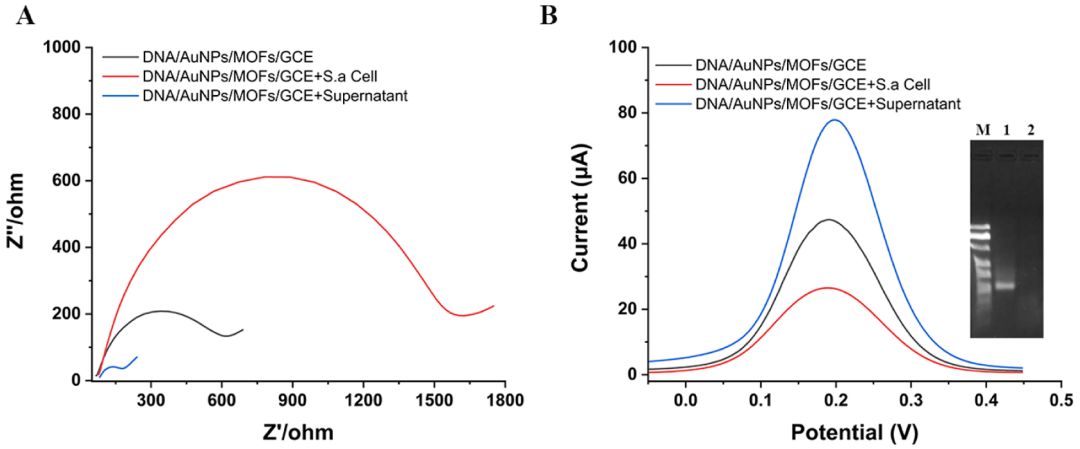

Figure 3. (A) EIS spectra and (B) DPV curves corresponding to the DNA/AuNPs/MOFs electrode incubated with or without *S. aureus*. Inset is agarose gel electrophoresis. (M: marker, 1: DNA aptamer, 2: DNA aptamer incubated with the *S. aureus* supernatant.)

RESULTS AND DISCUSSION

Characterization of MOF Films. The morphologies and structures of the synthesized Cu-MOF films on the electrode surface have been characterized by scanning electron microscopy (SEM). From Figure 1A, the morphology of cube crystals and the structure of layer upon layer can be clearly seen, indicating the gradual growth of Cu-MOFs on the electrode surface. After AuNPs are assembled further, the surfaces of MOFs become rough and surrounded by many nanoparticles, illustrating the successful synthesis on the external surface of Cu-MOFs (Figure 1B). Furthermore, the crystal structure of Cu-MOFs is shown in Figure 1C, where its 3D unit cells represent metal corners with are paddle-wheel-shaped connected by linkers. In order to validate that the Cu-MOFs deposited on the GCE electrode keep their structural integrity, powder X-ray diffraction (XRD) has also been performed, and the result is consistent with that obtained from simulation (Figure 1D).

Feasibility of the Biosensor. To investigate the feasibility of biosensor fabrication, the electrochemical properties of MOF films are first analyzed through EIS with a $[Fe(CN)_6]^{3-/4-}$ redox couple. As shown in Figure 2A, the bare GC electrode presents a semicircle diameter with an impedance value of almost 180 Ω (curve a). After the deposition of MOF films, the value of impedance decreased to 50 Ω (curve b) because of the high conductivity and positive metal ions of MOFs. With the assembly of AuNPs on the surface, the impedance spectrum is similar to a straight line (curve c), indicating that the composite nanomaterial may further improve the electron-transfer capability. Meanwhile, DPV is applied to observe the signal of $[Fe(CN)_6]^{3-/4-}$ more intuitively. From Figure 2B, it can be seen that the signals increased gradually after the bare electrode is modified with MOF films and AuNPs. These results confirm that the AuNPs/MOFs composite films have high electrical conductivity and can promote the electron transfer, which can be used as modified materials for the electrode to construct the electrochemical biosensor. The comparison of performance between AuNPs/MOF and AuNPs has also been performed and the experimental result is shown in Figure S1. MOFs used here not only improve the electron-transfer capability but also enable the electrode surface to load more AuNPs because of the larger surface area, which allow them to bind with more DNA aptamers to increase the biosensor sensitivity.

Then, EIS and DPV are employed to analyze the target bacteria supernatant and cells. As shown in Figure 3A, the electrode modified with DNA/AuNPs/MOFs exhibits an electron-transfer resistance of 560 Ω. However, after incubation with the supernatant of bacterial culture, the diameter of the semicircle obviously decreases compared to the

https://doi.org/10.1021/acs.analchem.1c01763
Anal. Chem. 2021, 93, 8994–9001

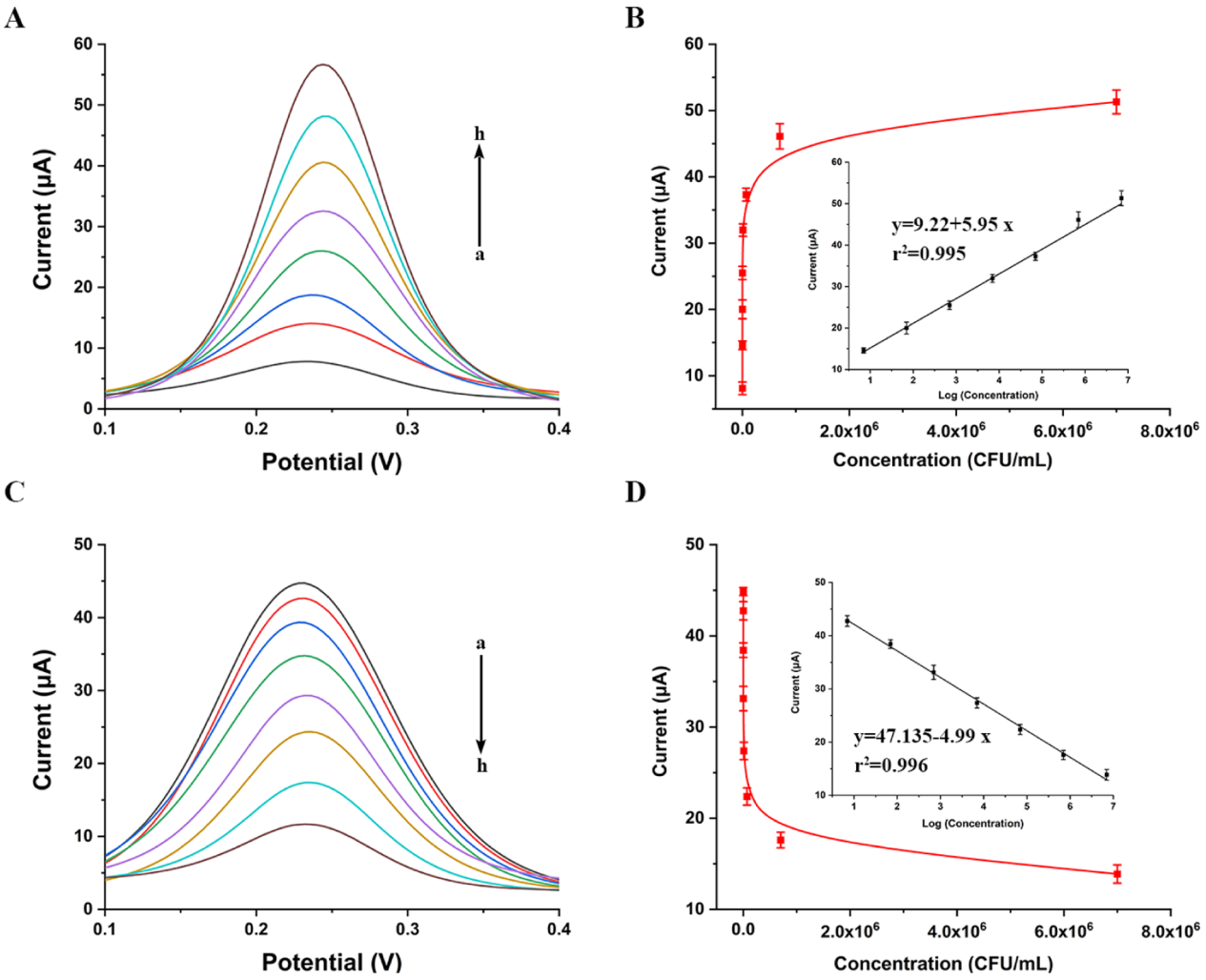

Figure 4. DPV curves recorded with different concentrations of (A) *S. aureus* supernatant and (C) *S. aureus* cells, a–h (cfu/mL): 0, 7, 7×10^1, 7×10^2, 7×10^3, 7×10^4, 7×10^5, and 7×10^6, respectively. (B,D) Values of peak current *vs S. aureus* concentrations. Inset is the linear range. Error bars represent the standard derivation of three independent experiments.

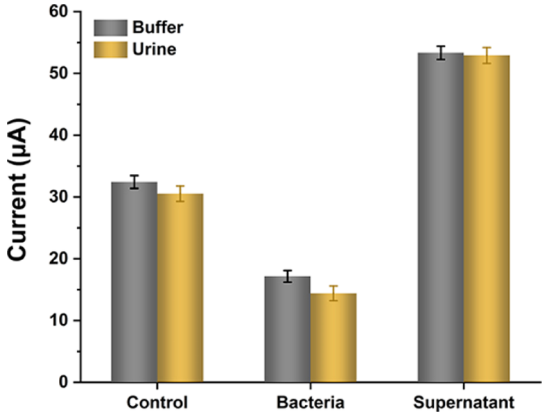

Figure 5. Corresponding DPV curves obtained by incubating with bacterial cells or supernatant in PBS or urine. Error bars represent the standard derivation of three independent experiments.

control, indicating that the interface impedance had decreased (Figure 3A). Due to the digestion of DNA aptamers by MNase, the amount of DNA on the electrode lessens; thus, the signal of $[Fe(CN)_6]^{3-/4-}$ obtained by DPV measurements in the solution increases (Figure 3B), which is consistent with our assumption. In addition, the feasibility of this biosensor was further verified by agarose gel electrophoresis analysis (Figure 3B, inset). Lines 1 and 2 are the DNA aptamer before and after incubation with the supernatant of *S. aureus*, respectively. It can be seen that line 1 exhibits an obvious band, while the band is not observed in line 2, which further proves that the degradation of DNA is triggered by MNase in the supernatant. On the other hand, when the target pathogen cells are employed by the DNA/AuNPs/MOFs sensing layer, the value of impedance significantly increased and almost reached 1500 Ω, suggesting the successful capture of the pathogen. The viability has been further verified by the DPV method. From Figure 3B, it can be seen that a much smaller signal is obtained in the presence of the target pathogen compared with the negative control. These results are attributed to the high insulating character and the negative charge of the pathogen, showing that the reaction is target-responsive.

Optimization of Experimental Conditions. To obtain the best performance of the biosensor, several relevant experimental conditions have been optimized. First, we optimized the deposition conditions of MOF films on the electrode surface by using CV according to relevant previous studies.[20,42] As shown in Figure S2A, when the electrode modified with MOF films is scanned by CV in 0.1 M KCl

https://doi.org/10.1021/acs.analchem.1c01763
Anal. Chem. 2021, 93, 8994–9001

Table 1. Detection of the *S. aureus* Supernatant and Cells in Urine (n = 3)

added (cfu/mL)	detected (cfu/mL)	RSD (%)	recovery (%)
7×10	$6.81 \pm 0.24 \times 10/7.21 \pm 0.27 \times 10$	3.52/3.74	97.2/103
7×10^3	$7.16 \pm 0.33 \times 10^3/7.45 \pm 0.36 \times 10^3$	4.60/4.83	102/106
7×10^5	$6.85 \pm 0.32 \times 10^5/6.77 \pm 0.31 \times 10^5$	4.67/4.57	97.8/96.7

solution, two pairs of redox waves are observed. These voltammetry behaviors are caused by the rapid redox-active sites of copper sites inside Cu-MOF films on the electrode surface, where the waves result from Cu^{2+}/Cu^{+} and Cu^{+}/Cu^{0}.[51−53] From the cyclic voltammogram, it is revealed that the current increases gradually with the higher applied potential. When the potential reaches −1.3 V, the current is almost stable, so we choose −1.3 V for the deposition and synthesis of the MOF film on the electrode. After that, the deposition time of the Cu-MOF films is optimized by using the same method. As shown in Figure S2B, at prolonged times, the MOF crystal particles formed on the electrode surface grow more, and the current increases and almost reaches a plateau at the deposition time of 5 min. Therefore,, 5 min is likely sufficient for the synthesis of MOF films.

After optimizing the deposition conditions of MOF films, the concentration of the DNA aptamer is optimized. First, AuNPs/MOFs/GCE is incubated with different concentrations of DNA aptamers at 37 °C for 30 min. As shown in Figure S3A, it is noticed that the currents decreased with the addition of the DNA aptamers and reached a stable level at 1 μM. Therefore, 1 μM is chosen as the optimal concentration for the detection of the *S. aureus* supernatant. Because the signal for the detection of *S. aureus* cells decreases with pathogen cells, the suitable concentration is chosen based on the difference before and after incubating with the pathogen. The modified electrode is incubated with the same amount of *S. aureus* and detected by DPV. As shown in Figure S4A, when the concentration of the DNA aptamer is 0.25 μM, the change is the highest, so 0.25 μM is selected as the optimal concentration. Then, we continue to optimize the incubation time of the target by detecting the $[Fe(CN)_6]^{3-/4-}$ signal in the solution. 10 μL of the supernatant of *S. aureus* is added onto the modified electrode to optimize the incubation time and 15 min is selected as the optimal incubation time (Figure S3B). Meanwhile, it can be seen that 30 min is sufficient to reduce the signal to a stable level by the *S. aureus* cells, so the reaction time is 30 min (Figure S4B).

Performance of the Biosensor. Under the optimized conditions, the performance of this biosensor is investigated by DPV measurements to detect the target pathogen. The content of *S. aureus* has been calculated by the plate counting method and diluting to different concentrations. First, 10 μL of the supernatant of *S. aureus* is used to investigate the performance of this biosensor. As shown in Figure 4A, as the concentration of *S. aureus* increases, more amount of MNase is secreted, more DNA sequences on the electrode surface get digested, and thus the electrochemical currents enhance gradually. According to the relationship between peak currents and the logarithmic values of *S. aureus* concentrations, a linear equation can be established ranging from 7 to 7×10^6 cfu/mL with $y = 9.22 + 5.95x$ ($r^2 = 0.995$) (Figure 4B), where y is the current of the DPV signal and x is the logarithm of the *S. aureus* concentration. The limit of detection (LOD) is calculated to be 1.9 cfu/mL on the basis of the lowest detected concentration being equal to the sum of the background signal plus three standard deviations. Then, the biosensor is further employed to directly analyze *S. aureus* by detecting bacterial cells. As shown in Figure 4C, the peak currents decrease with increasing the amount of microbial cells, and a linear relationship can be set up between the peak currents and the logarithmic values of *S. aureus* concentrations (Figure 4D). The LOD is calculated to be 5.2 cfu/mL according to the linear equation: $y = 47.135 - 4.99x$ ($r^2 = 0.996$). Although the LOD of this strategy is higher than that of the above method, the biosensor of this design can be used to detect other pathogens by simply replacing the DNA aptamer sequences, showing great universality for clinic diagnosis. The proposed method has also been compared with other reported methods, so our method shows a broader linear range and a lower LOD, indicating that this method can detect pathogens with satisfactory sensitivity (Table S1). Moreover, the designed platform not only supports a common method to detect pathogens through molecular recognition but also can continue to evaluate the pathogenicity by analyzing the MNase secreted by *S. aureus*.

Next, the selectivity of this platform is verified by detecting the supernatant and bacterial cells of *E. coli* (Gram-negative bacteria) as well as *L. monocytogenes* (Gram-positive bacteria), respectively (7×10^3 cfu/mL). As shown in Figure S5, since MNase is specifically secreted by *S. aureus*, the signal is enhanced only by incubating with the supernatant of *S. aureus*. Additionally, the signal is reduced just in the presence of *S. aureus* cells because of the specificity of the DNA aptamer. The currents of *E. coli* and *L. monocytogenes* showed almost no change, confirming the good selectivity during the detection of *S. aureus*. Additionally, due to the extreme heat stability of MNase,[54] the experiment of specificity has also been proved after incubating different samples at 100 °C for 20 min (Figure S6).

Real-Sample Analysis. In order to evaluate the sensor performance and the method validation in real samples, the supernatant and bacterial cells diluted with urine are challenged. From Figure 5, it can be seen that the currents of bacteria or supernatant diluted with PBS buffer or urine are almost the same, indicating the good anti-interference ability of the sensor. The different concentrations of *S. aureus* spiked in urine are also analyzed by the two approaches of our proposed method. The recovery rates range from 97.2 to 102, with admissible relative standard deviations (RSDs) of and 96.7 to 106%, respectively (Table 1). These results suggest that the currently developed biosensor works efficiently in complex biological samples, showing good selectivity, accuracy, and great potential application in clinical diagnosis.

CONCLUSIONS

In summary, an electrochemical biosensor designed by Cu-MOF thin films prepared by using electrochemical deposition has been successfully proposed. The newly developed biosensor could detect *S. aureus* by dual identification—analyze the S. aureus specifically secreted MNase in the supernatant as well as directly detect the bacterial cells through

https://doi.org/10.1021/acs.analchem.1c01763
Anal. Chem. 2021, 93, 8994−9001

the aptamer recognition—with good accuracy. Moreover, analysis of a noninvasive fluid spiked with the pathogen demonstrates that this platform has high selectivity and anti-interference ability in complex biological samples, proving its potential in clinical applications. In addition, this method can directly quantify the target bacteria without extra signal elements and thus is suitable for the timely and simple clinical detection. Since MNase is one of the pathogenic factors of *S. aureus*, this work may also be of great help to analyze the pathogenicity and mechanism of drug resistance of pathogenic bacteria.

■ ASSOCIATED CONTENT

Supporting Information

The Supporting Information is available free of charge at https://pubs.acs.org/doi/10.1021/acs.analchem.1c01763.

Experimental section; optimization of the deposition of MOF films and the conditions; selectivity and anti-interference ability of this biosensor; and comparison of this biosensor with those of previous methods (PDF)

■ AUTHOR INFORMATION

Corresponding Authors

Farid A. Harraz − *Promising Centre for Sensors and Electronic Devices (PCSED), Advanced Materials and Nano-Research Centre, Najran University, Najran 11001, Saudi Arabia; Nanomaterials and Nanotechnology Department, Central Metallurgical Research and Development Institute (CMRDI), Cairo 11421, Egypt*; Email: faharraz@nu.edu.sa

Genxi Li − *State Key Laboratory of Pharmaceutical Biotechnology, School of Life Sciences, Nanjing University, Nanjing 210023, P. R. China; Center for Molecular Recognition and Biosensing, School of Life Sciences, Shanghai University, Shanghai 200444, P. R. China*; orcid.org/0000-0001-9663-9914; Email: genxili@nju.edu.cn

Authors

Zhaowei Sun − *State Key Laboratory of Pharmaceutical Biotechnology, School of Life Sciences, Nanjing University, Nanjing 210023, P. R. China*

Ying Peng − *State Key Laboratory of Pharmaceutical Biotechnology, School of Life Sciences, Nanjing University, Nanjing 210023, P. R. China*

Minghui Wang − *State Key Laboratory of Pharmaceutical Biotechnology, School of Life Sciences, Nanjing University, Nanjing 210023, P. R. China*

Yuxin Lin − *State Key Laboratory of Pharmaceutical Biotechnology, School of Life Sciences, Nanjing University, Nanjing 210023, P. R. China*

Mohammed Jalalah − *Promising Centre for Sensors and Electronic Devices (PCSED), Advanced Materials and Nano-Research Centre, Najran University, Najran 11001, Saudi Arabia; Department of Electrical Engineering, Faculty of Engineering, Najran University, Najran 11001, Saudi Arabia*; orcid.org/0000-0002-6828-3874

Saeed A. Alsareii − *Department of Surgery, College of Medicine, Najran University, Najran 11001, Saudi Arabia*

Jie Yang − *State Key Laboratory of Pharmaceutical Biotechnology, School of Life Sciences, Nanjing University, Nanjing 210023, P. R. China*

Complete contact information is available at: https://pubs.acs.org/10.1021/acs.analchem.1c01763

Notes

The authors declare no competing financial interest.

■ ACKNOWLEDGMENTS

The authors extend their appreciation to the Deputyship for Research & Innovation, Ministry of Education in Saudi Arabia, for funding this research work through project number 875 and the support by the National Natural Science Foundation of China (grant no. 81772593).

■ REFERENCES

(1) Furukawa, H.; Cordova, K. E.; O'Keeffe, M.; Yaghi, O. M. *Science* **2013**, *341*, 1230444.

(2) Kreno, L. E.; Leong, K.; Farha, O. K.; Allendorf, M.; Van Duyne, R. P.; Hupp, J. T. *Chem. Rev.* **2012**, *112*, 1105−1125.

(3) Horcajada, P.; Chalati, T.; Serre, C.; Gillet, B.; Sebrie, C.; Baati, T.; Eubank, J. F.; Heurtaux, D.; Clayette, P.; Kreuz, C.; Chang, J.-S.; Hwang, Y. K.; Marsaud, V.; Bories, P.-N.; Cynober, L.; Gil, S.; Férey, G.; Couvreur, P.; Gref, R. *Nat. Mater.* **2010**, *9*, 172−178.

(4) Sun, Z.; Wu, S.; Ma, J.; Shi, H.; Wang, L.; Sheng, A.; Yin, T.; Sun, L.; Li, G. *ACS Appl. Mater. Interfaces* **2019**, *11*, 36316−36323.

(5) Duan, J.; Chen, S.; Zhao, C. *Nat. Commun.* **2017**, *8*, 15341.

(6) Han, X.; Hong, Y.; Ma, Y.; Lu, W.; Li, J.; Lin, L.; Sheveleva, A. M.; Tuna, F.; McInnes, E. J. L.; Dejoie, C.; Sun, J.; Yang, S.; Schröder, M. *J. Am. Chem. Soc.* **2020**, *142*, 15235−15239.

(7) Ma, X.; Chai, Y.; Li, P.; Wang, B. *Acc. Chem. Res.* **2019**, *52*, 1461−1470.

(8) Shekhah, O.; Liu, J.; Fischer, R. A.; Wöll, C. *Chem. Soc. Rev.* **2011**, *40*, 1081−1106.

(9) Bétard, A.; Fischer, R. A. *Chem. Rev.* **2012**, *112*, 1055−1083.

(10) Zhang, X.; Wan, K.; Subramanian, P.; Xu, M.; Luo, J.; Fransaer, J. *J. Mater. Chem. A* **2020**, *8*, 7569−7587.

(11) Stavila, V.; Talin, A. A.; Allendorf, M. D. *Chem. Soc. Rev.* **2014**, *43*, 5994−6010.

(12) D'Alessandro, D. M.; Kanga, J. R. R.; Caddy, J. S. *Aust. J. Chem.* **2011**, *64*, 718−722.

(13) Talin, A. A.; Centrone, A.; Ford, A. C.; Foster, M. E.; Stavila, V.; Haney, P.; Kinney, R. A.; Szalai, V.; El Gabaly, F.; Yoon, H. P.; Léonard, F.; Allendorf, M. D. *Science* **2014**, *343*, 66−69.

(14) Sheberla, D.; Sun, L.; Blood-Forsythe, M. A.; Er, S.; Wade, C. R.; Brozek, C. K.; Aspuru-Guzik, A.; Dincă, M. *J. Am. Chem. Soc.* **2014**, *136*, 8859−8862.

(15) Bhardwaj, S. K.; Bhardwaj, N.; Mohanta, G. C.; Kumar, P.; Sharma, A. L.; Kim, K.-H.; Deep, A. *ACS Appl. Mater. Interfaces* **2015**, *7*, 26124−26130.

(16) de Lourdes Gonzalez-Juarez, M.; Flores, E.; Martin-Gonzalez, M.; Nandhakumar, I.; Bradshaw, D. *J. Mater. Chem. A* **2020**, *8*, 13197−13206.

(17) Snyder, M. A.; Tsapatsis, M. *Angew. Chem., Int. Ed. Engl.* **2007**, *46*, 7560−7573.

(18) Shekhah, O.; Wang, H.; Zacher, D.; Fischer, R. A.; Wöll, C. *Angew. Chem., Int. Ed. Engl.* **2009**, *48*, 5038−5041.

(19) Shekhah, O.; Wang, H.; Paradinas, M.; Ocal, C.; Schüpbach, B.; Terfort, A.; Zacher, D.; Fischer, R. A.; Wöll, C. *Nat. Mater.* **2009**, *8*, 481−484.

(20) Li, M.; Dinca, M. *J. Am. Chem. Soc.* **2011**, *133*, 12926−12929.

(21) Mintova, S.; Bein, T. *Adv. Mater.* **2001**, *13*, 1880−1883.

(22) Stassen, I.; Styles, M.; Grenci, G.; Gorp, H. V.; Vanderlinden, W.; Feyter, S. D.; Falcaro, P.; Vos, D. D.; Vereecken, P.; Ameloot, R. *Nat. Mater.* **2016**, *15*, 304−310.

(23) Alizadeh, S.; Nematollahi, D. *J. Am. Chem. Soc.* **2017**, *139*, 4753−4761.

(24) Campagnol, N.; Van Assche, T. R. C.; Li, M.; Stappers, L.; Dincă, M.; Denayer, J. F. M.; Binnemans, K.; De Vos, D. E.; Fransaer, J. *J. Mater. Chem. A* **2016**, *4*, 3914−3925.

(25) Baker, S.; Thomson, N.; Weill, F. X.; Holt, K. E. *Science* **2017**, *360*, 733−738.

(26) Harris, S. R.; Feil, E. J.; Holden, M. T. G.; Quail, M. A.; Nickerson, E. K.; Chantratita, N.; Gardete, S.; Tavares, A.; Day, N.; Lindsay, J. A.; Edgeworth, J. D.; de Lencastre, H.; Parkhill, J.; Peacock, S. J.; Bentley, S. D. *Science* **2010**, *327*, 469−474.
(27) Marshall, B. M.; Levy, S. B. *Clin. Microbiol. Rev.* **2011**, *24*, 718−733.
(28) Turner, N. A.; Sharma-Kuinkel, B. K.; Maskarinec, S. A.; Eichenberger, E. M.; Shah, P. P.; Carugati, M.; Holland, T. L.; Fowler, V. G., Jr. *Nat. Rev. Microbiol.* **2019**, *17*, 203−218.
(29) Holden, M. T. G.; Hsu, L.-Y.; Kurt, K.; Weinert, L. A.; Mather, A. E.; Harris, S. R.; Strommenger, B.; Layer, F.; Witte, W.; de Lencastre, H.; Skov, R.; Westh, H.; Zemlickova, H.; Coombs, G.; Kearns, A. M.; Hill, R. L. R.; Edgeworth, J.; Gould, I.; Gant, V.; Cooke, J.; Edwards, G. F.; McAdam, P. R.; Templeton, K. E.; McCann, A.; Zhou, Z.; Castillo-Ramirez, S.; Feil, E. J.; Hudson, L. O.; Enright, M. C.; Balloux, F.; Aanensen, D. M.; Spratt, B. G.; Fitzgerald, J. R.; Parkhill, J.; Achtman, M.; Bentley, S. D.; Nubel, U. *Genome Res.* **2013**, *23*, 653−664.
(30) Tenover, F. C.; McDougal, L. K.; Goering, R. V.; Killgore, G.; Projan, S. J.; Patel, J. B.; Dunman, P. M. *J. Clin. Microbiol.* **2006**, *44*, 108−118.
(31) Hussain, S.; Joo, J.; Kang, J.; Kim, B.; Braun, G. B.; She, Z.-G.; Kim, D.; Mann, A. P.; Mölder, T.; Teesalu, T.; Carnazza, S.; Guglielmino, S.; Sailor, M. J.; Ruoslahti, E. *Nat. Biomed. Eng.* **2018**, *2*, 95−103.
(32) Lee, A. S.; de Lencastre, H.; Garau, J.; Kluytmans, J.; Malhotra-Kumar, S.; Peschel, A.; Harbarth, S. *Nat. Rev. Dis. Prim.* **2018**, *4*, 18033.
(33) Stokes, J. M.; Yang, K.; Swanson, K.; Jin, W.; Cubillos-Ruiz, A.; Donghia, N. M.; MacNair, C. R.; French, S.; Carfrae, L. A.; Bloom-Ackermann, Z.; Tran, V. M.; Chiappino-Pepe, A.; Badran, A. H.; Andrews, I. W.; Chory, E. J.; Church, G. M.; Brown, E. D.; Jaakkola, T. S.; Barzilay, R.; Collins, J. J. *Cell* **2020**, *180*, 688−702.
(34) Sun, Z.; Wu, S.; Peng, Y.; Wang, M.; Jalalah, M.; Al-Assiri, M. S.; Harraz, F. A.; Yang, J.; Li, G. *Chem. Eng. J.* **2021**, *405*, 126707.
(35) Jiang, N.; Wu, H.-T.; Lin, Q.-R.; Hu, Y.-J.; Yu, B. *J. Surg. Res.* **2020**, *247*, 356−363.
(36) Qiao, Y.; Liu, X.; Li, B.; Han, Y.; Zheng, Y.; Yeung, K. W. K.; Li, C.; Cui, Z.; Liang, Y.; Li, Z.; Zhu, S.; Wang, X.; Wu, S. *Nat. Commun.* **2020**, *11*, 4446.
(37) Li, H.-K.; Rombach, I.; Zambellas, R.; Walker, A. S.; McNally, M. A.; Atkins, B. L.; Lipsky, B. A.; Hughes, H. C.; Bose, D.; Kümin, M.; Scarborough, C.; Matthews, P. C.; Brent, A. J.; Lomas, J.; Gundle, R.; Rogers, M.; Taylor, A.; Angus, B.; Byren, I.; Berendt, A. R.; Warren, S.; Fitzgerald, F. E.; Mack, D. J. F.; Hopkins, S.; Folb, J.; Reynolds, H. E.; Moore, E.; Marshall, J.; Jenkins, N.; Moran, C. E.; Woodhouse, A. F.; Stafford, S.; Seaton, R. A.; Vallance, C.; Hemsley, C. J.; Bisnauthsing, K.; Sandoe, J. A. T.; Aggarwal, I.; Ellis, S. C.; Bunn, D. J.; Sutherland, R. K.; Barlow, G.; Cooper, C.; Geue, C.; McMeekin, N.; Briggs, A. H.; Sendi, P.; Khatamzas, E.; Wangrangsimakul, T.; Wong, T. H. N.; Barrett, L. K.; Alvand, A.; Old, C. F.; Bostock, J.; Paul, J.; Cooke, G.; Thwaites, G. E.; Bejon, P.; Scarborough, M. *N. Engl. J. Med.* **2019**, *380*, 425−436.
(38) Zhang, D.; Bi, H.; Liu, B.; Qiao, L. *Anal. Chem.* **2018**, *90*, 5512−5520.
(39) Bontron, S.; Poirel, L.; Nordmann, P. *J. Antimicrob. Chemother.* **2016**, *71*, 2318−2320.
(40) Akanda, M. R.; Tamilavan, V.; Park, S.; Jo, K.; Hyun, M. H.; Yang, H. *Anal. Chem.* **2013**, *85*, 1631−1636.
(41) Sun, Z.; Wang, L.; Wu, S.; Pan, Y.; Dong, Y.; Zhu, S.; Yang, J.; Yin, Y.; Li, G. *Anal. Chem.* **2020**, *92*, 3819−3826.
(42) Ji, L.; Wang, J.; Wu, K.; Yang, N. *Adv. Funct. Mater.* **2018**, *28*, 1706961.
(43) Arnone, A.; Bier, C. J.; Cotton, F. A.; Hazen, E. E.; Richardson, D. C.; Richardson, J. S. *Proc. Natl. Acad. Sci. U. S. A.* **1969**, *64*, 420.
(44) Lagacé-Wiens, P. R.; Alfa, M. J.; Manickam, K.; Karlowsky, J. A. *J. Clin. Microbiol.* **2007**, *45*, 3478.
(45) He, Y.; Xiong, L.-H.; Xing, X.-J.; Tang, H.-W.; Pang, D.-W. *Biosens. Bioelectron.* **2013**, *42*, 467−473.
(46) He, Y.; Jiao, B. *RSC Adv.* **2015**, *5*, 104116−104121.
(47) Yi, S. Y.; Jeong, J.; Kim, K. E.; Park, K.; Shin, Y. B. *ACS Infect. Dis.* **2020**, *6*, 215−223.
(48) Yang, L.; Bashir, R. *Biotechnol. Adv.* **2008**, *26*, 135−150.
(49) Furst, A. L.; Francis, M. B. *Chem. Rev.* **2019**, *119*, 700−726.
(50) Li, J.; Gao, T.; Gu, S.; Zhi, J.; Yang, J.; Li, G. *Biosens. Bioelectron.* **2017**, *87*, 352−357.
(51) Wu, L.; Lu, Z.; Ye, J. *Biosens. Bioelectron.* **2019**, *135*, 45−49.
(52) Shi, L.; Zhu, X.; Liu, T.; Zhao, H.; Lan, M. *Sens. Actuators, B* **2016**, *227*, 583−590.
(53) Duke, A. S.; Dolgopolova, E. A.; Galhenage, R. P.; Ammal, S. C.; Heyden, A.; Smith, M. D.; Chen, D. A.; Shustova, N. B. *J. Phys. Chem. C* **2015**, *119*, 27457−27466.
(54) Erickson, A.; Deibel, R. H. *Appl. Microbiol.* **1973**, *25*, 332−336.

https://doi.org/10.1021/acs.analchem.1c01763
Anal. Chem. 2021, 93, 8994−9001